PAPER

Comparison of the flows and radial electric field in the HSX stellarator to neoclassical calculations

To cite this article: A Briesemeister *et al* 2013 *Plasma Phys. Control. Fusion* **55** 014002

Plasma Phys. Control. Fusion **55** (2013) 014002 (5pp) doi:10.1088/0741-3335/55/1/014002

Comparison of the flows and radial electric field in the HSX stellarator to neoclassical calculations

A Briesemeister, K Zhai, D T Anderson, F S B Anderson and J N Talmadge

HSX Plasma Laboratory, University of Wisconsin-Madison, USA

E-mail: arbriesemeis@wisc.edu

Received 31 March 2012, in final form 27 June 2012
Published 17 December 2012
Online at stacks.iop.org/PPCF/55/014002

Abstract

Intrinsic flow velocities of up to $\sim$20 km s^{-1} have been measured using charge exchange recombination spectroscopy (CHERS) in the quasi-helically symmetric HSX stellarator and are compared with the neoclassical values calculated using an updated version (Lore 2010 *Measurement and Transport Modeling with Momentum Conservation of an Electron Internal Transport Barrier in HSX* (Madison, WI: University of Wisconsin); Lore *et al* 2010 *Phys. Plasmas* **17** 056101) of the PENTA code (Spong 2005 *Phys. Plasmas.* **12** 056114). PENTA uses the monoenergetic transport coefficients calculated by the drift kinetic equation solver code (Hirshman *et al* 1986 *Phys. Fluids* **29** 2951; van Rij and Hirshman 1989 *Phys. Fluids* B **1** 563), but corrects for momentum conservation. In the outer half of the plasma good agreement is seen between the measured parallel flow profile and the calculated neoclassical values when momentum correction is included. The flow velocity in HSX is underpredicted by an order of magnitude when this momentum correction is not applied. The parallel flow is calculated to be approximately equal for the majority hydrogen ions and the C^{6+} ions used for the CHERS measurements. The pressure gradient of the protons is the primary drive of the calculated parallel flow for a significant portion of the outer half of the plasma. The values of the radial electric field calculated with and without momentum correction were similar, but both were smaller than the measured values in the outer half of the plasma. Differences between the measured and predicted radial electric field are possibly a result of uncertainty in the composition of the ion population and sensitivity of the ion flux calculation to resonances in the radial electric field.

(Some figures may appear in colour only in the online journal)

1. Introduction

Measuring and modeling the radial electric field and plasma flow is important for understanding plasma transport and stability. Sheared flows driven by steep radial electric field profiles have been linked to reduced turbulent transport in both 'H-mode' plasmas and plasmas with internal transport barriers [6]. Flows have been shown to improve tolerance to magnetic field errors [7] and stabilize resistive wall modes [8] and neoclassical tearing modes [9]. Large, sheared parallel flows can destabilize a variety of modes because of the Kelvin–Helmholtz effect [10, 11]. The radial electric field can also reduce neoclassical particle transport, which is especially important in stellarators and other devices with significant non-symmetric magnetic field components. Non-axisymmetric fields exist in tokamaks because of the finite coil effects and have been intentionally introduced primarily for edge localized mode (ELM) suppression. Non-resonant magnetic perturbations in the DIII-D tokamak have been shown to cause a non-zero flow offset that can cause the plasma to spin without momentum injection from neutral beams [12].

A common method to calculate the flows and electric field in stellarators is to use the drift kinetic equation solver (DKES) code. DKES uses the incompressible flow approximation: $(\vec{E} \times \vec{B})/B^2 \approx (\vec{E} \times \vec{B})/\langle B^2 \rangle$, where $\langle\rangle$ denotes flux surface average. This approximation eliminates the changes in kinetic energy which would occur as a result of radial drift in the presence of E_r, making the drift

kinetic equation monoenergetic and allowing the use of a collision operator that only includes pitch angle scattering. This form of the drift kinetic equation has a non-physical singularity at the resonant value of the radial electric field: $E_r^{\rm res} = \pm(|m - (n/t)|/m)v_{{\rm T}a}B_\theta$ [13], where B_θ is the poloidal magnetic field, $v_{{\rm T}a}$ is the thermal velocity for species a, m and n are, respectively, the toroidal and poloidal mode numbers of the dominant component(s) of the magnetic field spectrum. For HSX, the dominant helical mode has $n = 4$ and $m = 1$. It has been shown that near a resonance in the radial electric field DKES does not correctly predict the particle diffusion coefficient [13]. This paper will focus on the outer half of the HSX plasma where E_r is predicted to be much smaller than the resonant value for the hydrogen ions.

The pitch angle scattering collision operator does not conserve momentum, with a result that DKES underpredicts the parallel flow in HSX. Three techniques [14–16] developed to correct the monoenergetic transport coefficients calculated by DKES to account for momentum exchange have been implemented in the current version of the PENTA code. All three techniques use the diffusion coefficients calculated by DKES, and are therefore not accurate near resonant values of E_r. The Sugama–Nishimura method was used for the calculations including momentum conservation shown in this paper.

2. The CHERS system

The charge exchange recombination spectroscopy (CHERS) system is used to measure the velocity, temperature, and density of C^{6+} ions in HSX. A 30 keV, 4 A, 3 ms diagnostic neutral beam [17] is fired radially through the plasma. The neutral beam does not cause any measurable perturbations to the electron temperature and density profiles. The Doppler shift, broadening and strength of the 529 nm emission line from C^{5+} ions is measured using two 0.75 m Czerny–Turner spectrometers. Electron multiplying ccds capture a series of images of the spectra during each discharge. Each image is integrated for 5 ms and read out in 1 ms. Images captured before and after the beam is fired are used to remove the background light. The spectral position of the emission line is measured during a series of shots with the magnetic field in the counter clockwise direction and compared with the position measured with the field in the clockwise direction. All components of the flow velocity should reverse when the field is reversed. Using the difference in the measured emission line position between the two cases effectively doubles the Doppler shift caused by the plasma velocity. This technique also eliminates systematic measurement error caused by the uncertainty in the relative strengths of the fine structure components of the emission line. A spectral calibration is performed after every shot using a neon calibration lamp to account for instrumental drift throughout the day.

The plasma profiles that will be used throughout the rest of this paper are shown in figure 2. The CHERS system measures C^{6+} density. Coronal equilibrium calculations and passive spectroscopic measurements indicate that significant

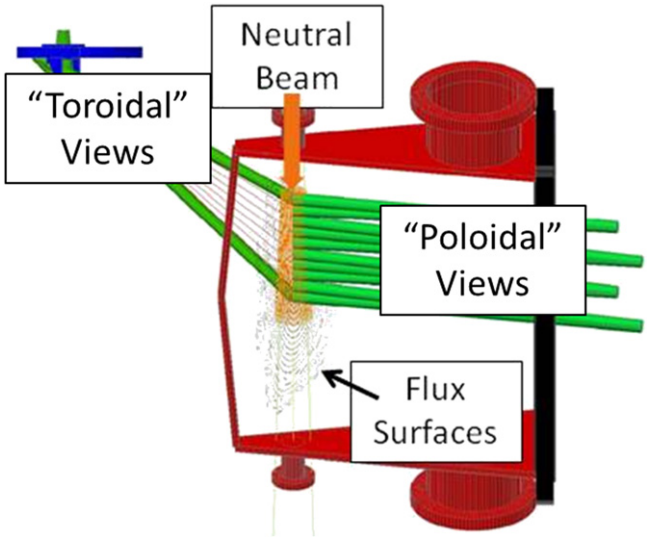

Figure 1. Drawing of the HSX CHERS system showing the neutral beam along with the viewing chords, the flux surfaces and a portion of the vacuum vessel.

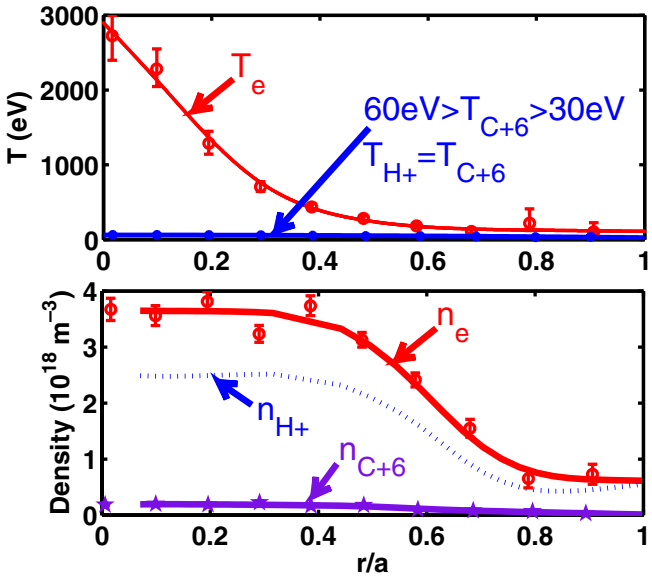

Figure 2. The electron temperature and density profiles were measured using Thomson scattering and used for the PENTA and DKES calculations. The C^{6+} temperature and density profiles were measured using the CHERS system. n_{H^+} is found by subtracting the C^{6+} charge density from n_e.

populations of lower ionization states of carbon are present, especially in the outer half of the plasma. Since no quantitative measurement of the density of the other ion species exists, an upper bound on the H^+ density is set by the difference between the electron density and the C^{6+} charge density, and used as an input for the neoclassical calculations. The flow velocity is measured at ten radial locations from two different directions as shown on the diagram in figure 1. One direction is a measurement of the flow in an approximately poloidal direction while the other is in an approximately toroidal direction. The views are not orthogonal. The two measurements provide constraints on the local flow velocity. A third constraint on

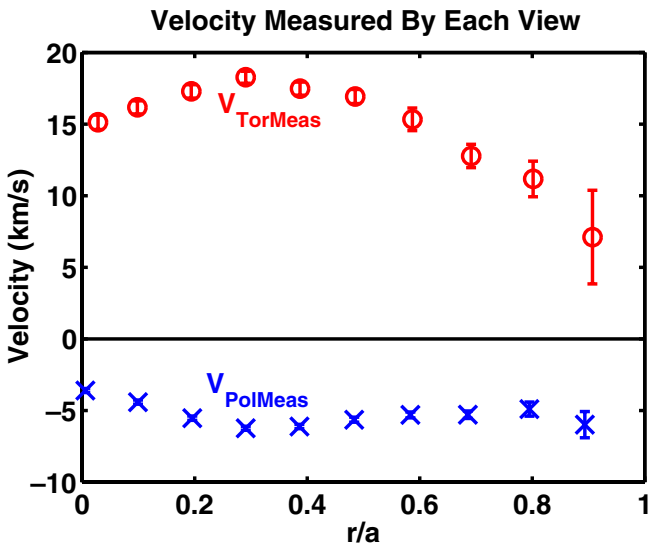

Figure 3. Flow velocity measured by each view shows that the flow velocity peaks around $r/a = 0.3$ with larger velocities measured by the approximately toroidal views than those measured by the approximately poloidal views.

the flow velocity vector is provided by the assumption that there will be no net flow in the $\nabla\Psi$ direction. The velocity measured by each view, shown in figure 3, is a beam density weighted average of the local flow velocity along the viewing direction throughout each beam/view intersection volume:

$$V_{\text{Measured}} = \frac{\iiint_{\text{View}} n_{\text{beam}} \vec{V}_{\text{local}} \bullet \hat{u}_{\text{view}}\, \text{dVolume}}{\iiint_{\text{View}} n_{\text{beam}}\, \text{dVolume}}.$$

Here n_{beam} is the local beam density, $\vec{V}_{\text{local}}$ is the local flow velocity and $\hat{u}_{\text{view}}$ is a unit vector along the view making the measurement. The C^{6+} density and emission coefficient are taken to be constant throughout each beam/view intersection volume. The local flow can be represented as the sum of a component parallel to the magnetic field and a component perpendicular to the magnetic field and $\nabla\Psi$. Using this representation the local flow velocity is $\vec{V}_{\text{local}} = V_{||}\hat{b} + V_{\perp}\hat{u}_{\perp}$ where $\hat{u}_{\perp} \equiv (\nabla\Psi \times \hat{b})/|(\nabla\Psi \times \hat{b})|$. The magnitude of the flow components ($V_{||}$ and $V_{\perp}$) are taken to be approximately constant throughout each poloidal/toroidal view pair. The geometric factor

$$G_{\text{View}||} \equiv \frac{\iiint_{\text{View}} n_{\text{beam}} \hat{b} \bullet \hat{u}_{\text{View}}\, \text{dVolume}}{\iiint_{\text{View}} n_{\text{Beam}}\, \text{dVolume}}$$

is used to describe the relationship between the velocity measured by each view and the flow parallel to the magnetic field lines. The geometric factor ($G_{\text{View}\perp}$) for the perpendicular direction is found by replacing $\hat{b}$ with $\hat{u}_{\perp}$. The geometric factors cannot properly account for the significant flow direction changes predicted throughout the core views of the plasma, since the beam/view intersection is relatively large when compared with the shape and size of the flux surfaces in the core of the plasma. In the outer half of the plasma changes in the flow velocity direction throughout each view volume should be small. The parallel and perpendicular flow components are found from the measured velocities by inverting the following relationship:

$$\begin{bmatrix} G_{\text{TorView}||} & G_{\text{TorView}\perp} \\ G_{\text{PolView}||} & G_{\text{PolView}\perp} \end{bmatrix} \begin{bmatrix} V_{||} \\ V_{\perp} \end{bmatrix} = \begin{bmatrix} V_{\text{TorMeas}} \\ V_{\text{PolMeas}} \end{bmatrix}.$$

V_{TorMeas} and V_{PolMeas} are the velocities measured by the toroidal and poloidal views at a radial location. The local value of E_r is related to $V_{\perp}$ using the radial force balance equation:

$$\vec{E}_{r\text{Local}} = \frac{1}{q_{C^{6+}} n_{C^{6+}}} \nabla p_{C^{6+}} - \vec{V}_{C^{6+}} \times \vec{B}.$$

The diamagnetic flow for C^{6+} is calculated from the CHERS measurements of the C^{6+} density and temperature and removed from the perpendicular flow to find the local E_r. The diamagnetic flow of C^{6+} is relatively small ($\lesssim 0.5\,\text{km}\,\text{s}^{-1}$) when compared with the diamagnetic flow for the protons ($\lesssim 3\,\text{km}\,\text{s}^{-1}$) because of the carbon's higher charge. The local $E_{r\text{Local}} = -\nabla\Phi$ is divided by the local value of ∇r_{PENTA} averaged over the view, where $r_{\text{PENTA}} \equiv \sqrt{\Psi/\pi B_{\text{o}}}$. This converts $E_{r\text{Local}}$ into the flux surface quantity $\langle E_r \rangle = -(\partial\Phi/\partial r_{\text{PENTA}})$ which is the quantity calculated by PENTA. The parallel flow term calculated by PENTA is the flux surface quantity $\langle V_{||\text{i}} B\rangle/\langle B^2\rangle$. In the region where the measurements are made the Pfirsch–Schlüter flows are predicted to make an insignificant contribution to the measured $V_{||}$, so the local $V_{||}$ values are converted to the flux surface quantity using the relationship: $V_{||\text{Local}} = (\langle V_{||\text{i}} B\rangle/\langle B^2\rangle) B_{\text{local}}$.

3. Momentum conservation must be enforced to correctly predict parallel flow in HSX

PENTA calculates the neoclassical particle fluxes as functions of the radial electric field for a set of surfaces within the plasma. In magnetic configurations with non-symmetric magnetic field components the particle fluxes are not intrinsically ambipolar and the radial electric field can be determined using the ambipolarity condition: $\sum_s Z_s \Gamma_s(E_r) = \Gamma_{\text{e}}(E_r)$. The radial electric field, along with the pressure gradient, drive flow perpendicular to the magnetic field direction. A flow parallel to the magnetic field can arise as a result of the plasma viscosity. HSX was optimized for quasi-helical symmetry. This helical direction of quasi-symmetry reduces flow damping [18] along the helical direction, allowing significant parallel flows to arise. DKES, which uses a non-momentum conserving collision operator, underpredicts the parallel flow in HSX by an order of magnitude, as shown in figure 4. Reasonable agreement is seen between the measured parallel flow and the parallel flow predicted by PENTA when momentum conservation is included. This demonstrates the importance of including momentum conservation when calculating plasma flow.

As shown in figure 5 the radial electric field profile measured by CHERS in this region is positive and larger than the E_r predicted by DKES or PENTA. This disagreement is possibly caused by neglecting the other ionization states of carbon and overestimating the proton density in the calculations. The measured value of E_r is very close to the resonant value of the carbon ions. In the calculations shown, the proton flux was much larger than the C^{6+} flux, reducing the

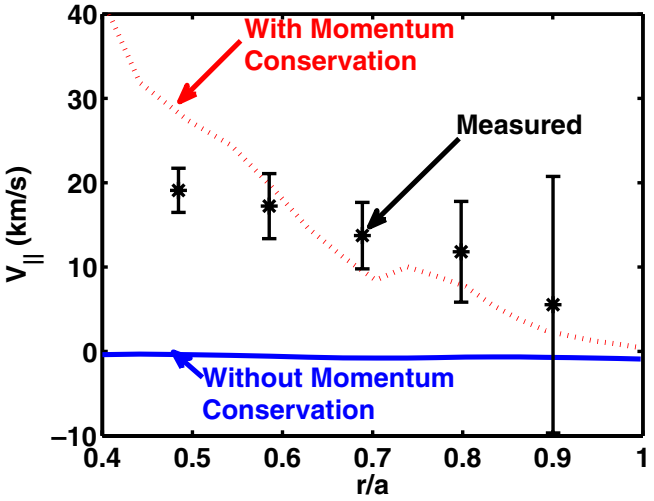

Figure 4. The asterisks (*) show the $V_\parallel$ measured by the CHERS system which is in reasonable agreement with the $V_\parallel$ predicted by PENTA including momentum conservation (dotted line). The solid line shows the much smaller value of $V_\parallel$ predicted by DKES without momentum conservation.

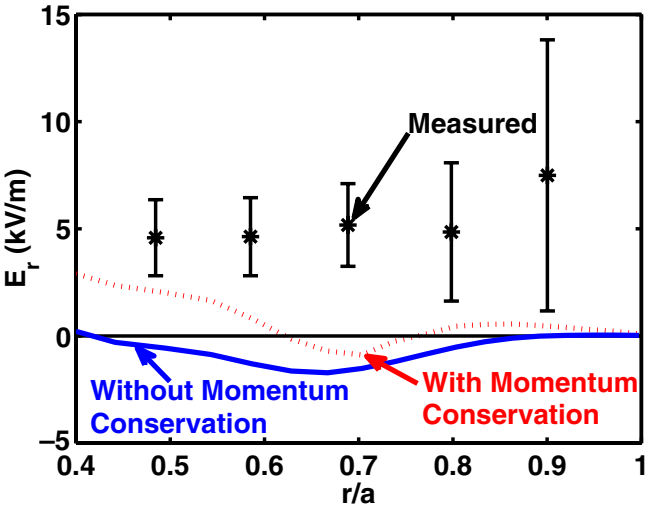

Figure 5. The asterisks (*) show the E_r measured using the CHERS system which is larger than the E_r profiles predicted by PENTA including momentum conservation (dotted line) and DKES without momentum conservation (solid line).

impact that inaccuracies in the C^{6+} flux near the resonance have on the calculated values of E_r. These inaccuracies near the carbon resonance will have a larger effect on the calculations if the total carbon density is included, necessitating the use of a calculation technique which can correctly calculate fluxes near resonances.

The parallel momentum balance equation

$$\frac{1}{\langle B^2\rangle}\sum_b\left(\delta_{ab}\begin{bmatrix} M_{a1} & M_{a2} \\ M_{a2} & M_{a3}\end{bmatrix}-\begin{bmatrix} l_{11}^{ab} & l_{12}^{ab} \\ l_{21}^{ab} & l_{22}^{ab}\end{bmatrix}\right)\begin{bmatrix} \langle Bu_{||b}\rangle \\ \frac{2}{5p_b}\langle Bq_{||b}\rangle\end{bmatrix} = \begin{bmatrix} N_{a1} & N_{a2} \\ N_{a2} & N_{a3}\end{bmatrix}\begin{bmatrix} X_{a1} \\ X_{a2}\end{bmatrix}$$

[14] is used in the current version of PENTA to calculate the parallel ion flow (in the original version only a single ion species could be included in the calculation). In this equation 'a' is used to indicate the ion species of interest and the summation is performed over all the ion species. The friction coefficients l_{ij}^{ab} are defined in [19]. The viscosity coefficients M_{ab}^{ij} and N_{ab}^{ij} are defined in [14] as functions of the monoenergtic transport coefficients calculated by DKES. The thermodynamic drives are $X_{a1} = -p_a'/n_a + q_a E_r$ and $X_{a2} = -T_a'/n_a$, where prime denotes a derivative in the radial direction. Since only electron heating is used in HSX the ion temperature and its gradient are small, making the X_{a2} term small. The parallel flow is determined primarily by the X_{a1} drive term. Figure 6 shows the pressure gradient component makes a significant contribution to the X_{a1} drive term of H^+. For the high charge state of C^{6+} the $q_a E_r$ component becomes dominant. The most notable difference between the drive terms of the two species is that they have opposite signs at $r/a \sim 0.7$. In the absence of frictional coupling the two ion species would have been predicted to flow at very different velocities and even in opposite directions near $r/a \sim 0.7$. PENTA calculations show that because the ions are collisional, all the species will have approximately the same $V_\parallel$ (differences were calculated to be $<0.2\,\mathrm{km\,s^{-1}}$). For the case shown the H^+ density is significantly higher than the C^{6+} density, causing the momentum transfer from H^+ to C^{6+} to be more efficient than the transfer from C^{6+} to H^+. The dominance of H^+ in determining the calculated parallel flow can be seen in figure 4 where $V_\parallel$ for C^{6+} ions predicted by PENTA remains positive for $r/a \sim 0.7$ despite the reversal of the sign of the C^{6+} drive term. This highlights the need to more accurately determine the composition of the ion population in the plasma since the H^+ population, and therefore its frictional coupling with the parallel flow of C^{6+}, is almost certainly lower than that used in the calculation.

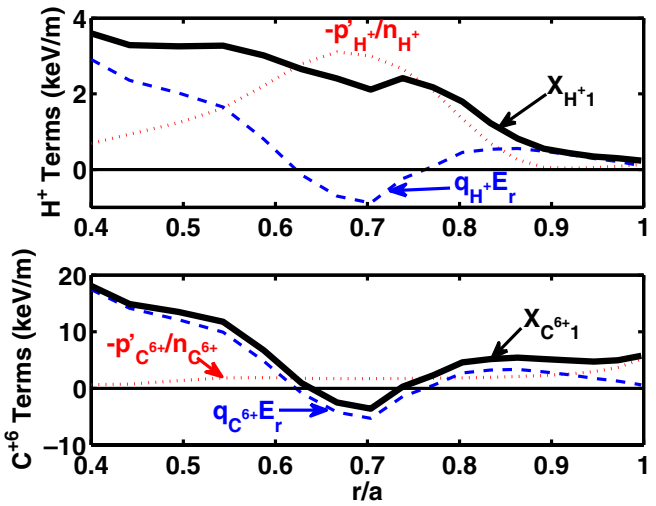

Figure 6. The dotted lines show the pressure gradient component, the dashed lines show the radial electric field component and the solid line shows the total thermodynamic drive term for each ion species for the outer half of the plasma. The H^+ drive term is dominated by the pressure gradient while the C^{6+} drive term is primarily determined by E_r because of the higher charge of C^{6+}.

4. Summary and discussion

Reasonable agreement is seen between the measured and neoclassically predicted parallel flow velocity in the outer half of the plasma when the effects of momentum conservation are included in the calculation. The fact that the parallel flow was underpredicted by an order of magnitude when momentum conservation was not included demonstrates the importance of including momentum conservation when calculating parallel flows in quasi-symmetric devices. The ability to model non-symmetric magnetic configurations and the inclusion of momentum conservation makes PENTA, applicable to devices with any level of symmetry. These include ideal tokamaks, tokamaks with resonant magnetic perturbation coils that slightly break the axisymmetry at the plasma edge, quasi-symmetric stellarators and finally, conventional stellarators.

At the same time, this paper highlights the need for further improvements in the neoclassical modeling for certain experimental conditions. In experiments such as HSX, where first harmonic electron cyclotron resonant heating and a 1.0 T magnetic field is used, density is limited to a relatively low value ($n_{e0} \sim 4 \times 10^{12}$ cm^{-3}) allowing the electron temperature to be much greater than the ion temperature in the plasma core, as seen in figure 2. Similar experimental conditions have been observed in W7-AS [20]. This temperature disparity can give rise to a large radial electric field, which causes the monoenergetic approximation used in DKES to become invalid. For plasmas with significant impurity content the resonance can become a concern even at lower values of E_r because more massive impurity ions will have lower thermal velocities and will be resonant at lower values of E_r. This is what occurs at the edge of HSX where the radial electric field is below the resonant value of the protons, but comparable to the resonant value of the carbon ions. A comparison with the results of a δf Monte Carlo code that does not employ the monoenergetic approximation would be useful in better understanding the broader applicability of the PENTA code. A full examination of these challenges is beyond the scope of this paper.

References

[1] Lore J 2010 *Measurement and Transport Modeling with Momentum Conservation of an Electron Internal Transport Barrier in HSX* (Madison, WI: University of Wisconsin)

[2] Lore J *et al* 2010 Internal electron transport barrier due to neoclassical ambipolarity in the helically symmetric experiment *Phys. Plasmas* **17** 056101

[3] Spong D A 2005 Generation and damping of neoclassical plasma flows in stellarators *Phys. Plasmas.* **12** 056114

[4] Hirshman S P, Shaing K C, van Rij W I, Beasley C O and Crume E C 1986 Plasma transport coefficients for nonsymmetric toroidal confinement systems *Phys. Fluids* **29** 2951

[5] van Rij W I and Hirshman S P 1989 Variational bounds for transport coefficients in three-dimensional toroidal plasmas *Phys. Fluids* B **1** 563

[6] Fujisawa A 2003 Experimental studies of structural bifurcation in stellarator plasmas *Plasma Phys. Control. Fusion* **45** R1–88

[7] Boozer A H 1996 Shielding of resonant magnetic perturbations by rotation *Phys. Plasmas* **3** 4620–7

[8] Garofalo A M *et al* 2007 Stability and control of resistive wall modes in high beta, low rotation DIII-D plasmas *Nucl. Fusion* **47** 1121–30

[9] Buttery R J *et al* 2008 The influence of rotation on the β_N threshold for the 2/1 neoclassical tearing mode in DIII-D *Phys. Plasmas* **15** 056115

[10] Chu M S 1998 Shear flow destabilization of a slowly rotating tokamak *Phys. Plasmas* **5** 183–91

[11] Kinsey J E, Waltz R E and Candy J 2005 Nonlinear gyrokinetic turbulence simulations of $E \times B$ shear quenching of transport *Phys. Plasmas* **12** 062302

[12] Garofalo A M *et al* 2008 Observation of plasma rotation driven by static nonaxisymmetric magnetic fields in a tokamak *Phys. Rev. Lett.* **101** 195005

[13] Beidler C D *et al* 2007 *ICNTS-Impact of Incompressible E×B Flow in Estimating Mono-Energetic Transport Coefficients*

[14] Sugama H and Nishimura S 2002 How to calculate the neoclassical viscosity, diffusion, and current coefficients in general toroidal plasmas *Phys. Plasmas* **9** 4637

[15] Maaßberg H, Beidler C D and Turkin Y 2009 Momentum correction techniques for neoclassical transport in stellarators *Phys. Plasmas* **16** 072504

[16] Taguchi M 1992 A method for calculating neoclassical transport coefficients with momentum conserving collision operator *Phys. Fluids* B **4** 3638

[17] Abdrashitov G F *et al* 2001 A diagnostic neutral beam system for the MST reversed-field pinch *Papers from the 13th Topical Conf. on High Temperature Plasma Diagnostics [Internet] (Tuscon, AZ)* (New York: AIP) pp 594–7 (cited 2010 Jan 12) Available from: http://link.aip.org/link/ ?RSI/72/594/1

[18] Gerhardt S P, Talmadge J N, Canik J M and Anderson D T 2005 Measurements and modeling of plasma flow damping in the helically symmetric experiment *Phys. Plasmas* **12** 056116

[19] Hirshman S P and Sigmar D J 1981 Neoclassical transport of impurities in tokamak plasmas *Nucl. Fusion.* **21** 1079–201

[20] Baldzuhn J, Kick M, Maassberg H and Team the W-A 1998 Measurement and calculation of the radial electric field in the stellarator W7-AS *Plasma Phys. Control. Fusion* **40** 967–86